Check for updates

JGR Planets

RESEARCH ARTICLE
10.1029/2019JE005984

Key Points:
- Cryomagmatic processes that occur under the conditions in Europa's upper crust are modeled through experimental petrology
- Different experiments reveal the importance of the initial composition and the evolution of volatiles during cooling and reheating
- Experimental findings (polymineralogy, metastability, and differentiation) help relate cryomagmatism to geological features on the surface

Supporting Information:
- **Figure S1**. Raman spectra of the ring breathing mode of cyclohexane at temperatures down to 263 K. The peaks are fitted to Lorentzian curves in order to obtain the Raman peak position as indicated in the figure for each spectrum.
  Figure S2. Raman spectra and the calibration curve used to quantify the changes in the sulfate concentration during the runs. The evolution of the fluids is also monitored spectroscopically. When $MgSO_4$ is dissolved in water, the main characteristic Raman signal of the salt is the symmetric stretching mode υ1 of the SO_4^{2-} molecule that appears at 980 cm^{-1} (Rudolph et al., 2003). To control the sulfate concentration in the aqueous fraction of cryomagmas with the composition of the ternary system H_2O-CO_2-$MgSO_4$ (Runs 3 – 6) along their P–T paths, we performed a previous calibration with six $MgSO_4$ aqueous solutions at 5, 10, 15, 20, 25 and 30 wt%. The salt concentration is estimated by the area ratio (AR = A(SO_4^{2-})/A(H_2O)) between the SO_4^{2-} peak, which is fitted to a Lorentzian curve, and the characteristic O-H symmetric stretch broad band of liquid water at 2700 – 4000 cm^{-1} is fitted to three Lorentzian curves (Walrafen et al., 1986). The adjustment of the area ratios and the salt concentrations result in a second-degree correlation curve, as shown at the top of the graph.
  Figure S3. Raman spectra of the sapphire window located at the top of the high-pressure chamber at different temperatures. Spectra taken with the chamber filled with air at 0.1 MPa. The characteristic signals of the

©2019. American Geophysical Union. All Rights Reserved.

Experimental Petrology to Understand Europa's Crust

V. Muñoz-Iglesias[1], O. Prieto-Ballesteros[1], and I. López[2]

[1]Centro de Astrobiología (CSIC-INTA), Torrejón de Ardoz, Spain, [2]Departamento de Biología, Geología, Física y Química Inorgánica, Universidad Rey Juan Carlos, Móstoles, Spain

Abstract The Jovian moon Europa is a prime target for astrobiology. A global subsurface water ocean and a geologically young surface provide evidence of an active planetary body with a potential deep habitable environment. Tectonism and cryomagmatism are both agents of resurfacing, with structures on the surface spatially related to reddish non-icy materials that could represent crystallized volatile and salt-rich fluids from the interior, possibly from the ocean or shallower aqueous bodies. Cryomagmatism could therefore be a mechanism for exposing the underlying liquid layers to the surface and could hold paramount importance for understanding the physical and chemical evolution of fluids during their ascent and emplacement and their connection with geological features at the surface. With these premises, we perform a set of laboratory experiments simulating the evolution of different fluids under the conditions in Europa's crust. These experiments allow us to constrain the physico-chemical and textural changes experienced by the different fluids and solids that are potentially emplaced within the icy crust and determine how they are affected by such secondary processes as reheating, melting, and ultimate recrystallization (e.g., in response to the emplacement of a second diapir close to the first one or tidal reheating). Based on these experimental results, we explore the connection of cryomagmas and their evolution near the surface to geologic features present on Europa's surface, such as pits, uplifts/domes, and microchaos regions, as well as the link with explosive cryovolcanism responsible for putative plumes at Europa.

Plain Language Summary The presence of an internal ocean and a geologically young surface on Europa is evidence that the planetary body is still active and consequently has a potential deep habitable environment. The moon's surface is continuously being renovated by tectonic deformation and cryomagmas that reach the surface. Different structures on the surface are associated with non-icy materials that could come from near the surface or the underlying ocean. Cryomagmatism could therefore be a mechanism for exposing materials from Europa's interior to the surface. To understand this process, we designed a set of laboratory experiments simulating the evolution of fluids of different compositions under the conditions of Europa's crust. These experiments allow us to study the physico-chemical behavior, geochemical evolution, and the associated textures after the different fluids cool when they ascend and are emplaced in the crust. We also test how they are affected by such secondary processes as reheating, melting, and final recrystallization. Based on these experimental results, we also explore the relationship of cryomagmas and their evolution to structures that we observe on Europa's surface, such as pits, uplifts, and chaos regions, and to the possibility of explosive eruptions and the formation of large volcanic plumes.

1. Introduction

Europa, Jupiter's icy satellite, has been of major astrobiological interest ever since data obtained during the Galileo mission revealed that it is a differentiated body with an icy crust overlying a water ocean in direct contact with a silicate mantle (Anderson, 1998; Kivelson et al., 2000). Europa has few impact craters, which is indicative of a young surface (40–90 Myr; Bierhaus et al., 2009 and references therein) and is possibly due to the geological activity that has recently resurfaced the moon. This resurfacing may still be taking place today.

The pervasive tectonic features, including ridges and faults, likely formed via extensional and shear mechanisms (Craft et al., 2016; Greenberg et al., 1998; Han & Showman, 2008; Head et al., 1999; Kadel et al., 1998; Prockter & Patterson, 2009) and could connect deep underlying materials with the surface (e.g., Craft et al., 2016; Culha & Manga, 2016; Manga & Michaut, 2017).

sapphire (Kadleíková et al., 2001), the O_2 (1555 cm^{-1}) and the N_2 (2330 cm^{-1}) of the air inside the chamber are also observed. At higher frequencies, the baseline is distorted by fluorescence caused by impurities.**Figure S4**. Full sequence of the pictures taken during the runs. The blue and orange lines represent cooling and heating, respectively.

Correspondence to:
V. Muñoz-Iglesias,
vmunoz@cab.inta-csic.es

Citation:
Muñoz-Iglesias, V., Prieto-Ballesteros, O., & López, I. (2019). Experimental Petrology to Understand Europa's Crust. *Journal of Geophysical Research: Planets*, *124*, 2660–2678. https://doi.org/10.1029/2019JE005984

Received 1 APR 2019
Accepted 22 SEP 2019
Published online 31 OCT 2019

Cryomagmatism is also a major agent of resurfacing. Pits, domes, spots, and microchaos are ubiquitous circular to elliptical features that are 7–15 km in diameter and separated by distances between 5 and 20 km (e.g., Greenberg et al., 2003; Head & Pappalardo, 1999). They are grouped under the term lenticulae in some works (for a discussion on the nomenclature of these features, see Greenberg et al., 2003), and they are interpreted as sites of intrusive and extrusive processes that occur at a low temperature (Collins et al., 2000; Figueredo et al., 2002; Greenberg et al., 2003; Pappalardo & Barr, 2004; Quick & Marsh, 2016; Culha & Manga, 2016; Marsh et al., 2017; Quick et al., 2017). Larger "chaotic terrains" define areas where surface materials have been fractured into discrete polygons with evidence of displacement (Carr et al., 1998; Greenberg et al., 1998) and are interpreted as areas where the brittle crust has been broken over a local mobile substrate (Collins et al., 2000; Schmidt et al., 2011). The recent discovery of possible volcanic plumes at Europa's southern hemisphere suggests the existence of current cryovolcanism on Europa (Arnold et al., 2019; Jia et al., 2018; Roth et al., 2014; Sparks et al., 2017).

Cryomagmatic structures are thought to form via diapiric processes that take place in Europa's crust. Nevertheless, since water ice is less dense than liquid water, cryomagmas would have difficulty reaching the surface. In addition, thermal diapirism seems insufficient when accounting for their formation (Pappalardo & Barr, 2004), suggesting that factors such as composition of the cryomagmas, specifically the presence of volatiles (Fagents et al., 2000; Muñoz-Iglesias et al., 2014), together with pressure-driven ascent, play important roles in their ascent through the crust. Thus, the low-temperature petrology and the chemical and physical behavior of fluids under the conditions of the upper crust are key to understanding the tectonics and magmatism on Europa.

Some indications regarding the chemistry of endogenous compounds have been obtained from the spectroscopic study of materials that have reached the surface. The study of the surface composition with Galileo's Near Infrared Mapping Spectrometer revealed that the magmatic and tectonic features on the surface are spatially associated with red materials that differ from the dominant surface water ice and are potentially related to the underlying ocean (Carlson et al., 1996; Fink et al., 1973; Johnson & McCord, 1971; Pilcher et al., 1972). Studies of the infrared spectra of these red materials suggest that they are likely the result of a mixture of salts with a proportion of sulfate hydrates or hydrated sulfuric acid, depending on the radiated hemisphere (Dalton et al., 2005; Dalton et al., 2013; McCord et al., 1998; McCord et al., 1999; Orlando et al., 2005). On the other hand, ground-based observations and experimental spectroscopic comparison studies (Brown & Hand, 2013; Fischer et al., 2016; Trumbo et al., 2017) strongly support chlorine salts as additional candidates for being part of the composition of the reddish materials (Hand & Carlson, 2015; Hanley et al., 2014). Although the experimental work presented in this paper is performed considering only sulfates and CO_2, the presence of other salts is evaluated in Section 4. On the other hand, the volatiles CO_2 and SO_2 have been detected. While CO_2 is associated with reddish materials, SO_2 has a sparse distribution (Hansen & McCord, 2008).

A constructive method of studying the roles of the composition and the presence of volatiles in the evolution of endogenous fluids is to experimentally reproduce the cryogenic petrology under the conditions of the Europan crust. In this work, we describe a series of laboratory experiments designed to determine the physical and chemical evolution of different fluids in their ascent through the crust to their emplacement at the upper layers close to the surface. Such experimental systems reveal the range of processes that operate on icy moons and whose understanding will be of great importance for the correct interpretation of the returned data from future missions to Europa (e.g., JUICE [JUpiter ICy moons Explorer] and Europa Clipper).

Our experimental setup allows us to evaluate the different processes that a fluid can experience during its evolution through the crust to its final emplacement at the upper layers of the moon close to the surface and to determine how these events can be noted at the surface. The experiments were conducted using an aqueous solution with gases dissolved at temperatures down to 267 K and pressures up to 3.5 MPa on average. All pressure-temperature (P-T) changes, which were either promoted during the experiment or due to the intrinsic properties of the sample, were recorded during the runs. The experiments were also monitored optically and via Raman spectroscopy. As fluids, we used one composed of pure H_2O and another composed of an aqueous solution of $MgSO_4$ at 15 wt%. In both cases, we added CO_2 to the solution in accordance with the spectroscopic observation of reddish materials on the surface. It is well-known that at

Table 1
Protocol Applied in Each Run to Explore Different Potential Paths That a Cryomagma Can Follow in Europa's Crust

Steps during the experiments						
Runs	Systems	1st CO_2 addition Duration (days)	Temperature (K)	2nd Cooling to 267 K Temperature of solid formation (stop CO_2 addition + stirring) (K)	3rd Heating Maximum temperature (K)	4th 2nd cooling to 267 K
1	H_2O–CO_2	7	282	278	273	Done
2		7	295	269	278	Done
3	H_2O–CO_2–$MgSO_4$	3	282	273	280	Done
4		7	282	270	274	Done
5		8	295	267	281	Not done
6		6	282	267	292	Done, followed by depressurization

Note. In Run 1, the second cooling is started before the complete melting of the solids. In Runs 2 and 5, CO_2 gas is added at 295 K. In Run 3, the system is heated not only to reach the melting temperature but also to achieve CO_2 exsolution. Run 5 is performed with the gas open until the end of the experiment and without a second cooling.

low temperatures, these systems lead to the stabilization of water ice, clathrate hydrates, and hydrated sulfates. The proportions among the minerals formed depend on the original chemical composition of the fluid and on the P-T conditions that each mineral stabilizes at (Kargel, 1991; Muñoz-Iglesias et al., 2014; Prieto-Ballesteros et al., 2005).

We therefore describe the pressure-temperature-time (P-T-t) paths followed for each fluid and explain the resulting textures in solids, as well as the Raman spectra obtained during their chemical and physical evolution. Finally, based on our experimental observations, we discuss how the emplacement of cryomagmas in Europa's shallow subsurface could be related to some geological structures observed at the surface.

2. Materials and Methods

The formation and evolution of different fluids under Europa's subsurface conditions have been simulated in the laboratory. The experimental setup includes a thermostatically controlled high-pressure chamber that allows extrapolation of the data to Europa's conditions (Muñoz-Iglesias et al., 2013). A circulation Thermostat Unistat 815 w (Huber, Germany) instrument is used to modify the sample temperature. The high-pressure chamber is placed in a vertical position, while the cell is connected to a tank of CO_2 (gas) via high-pressure tubing. It is equipped with a sapphire window (Roditi International, UK) that is 37 mm (diameter) × 10 mm (thickness) at the top in order to visually and spectroscopically monitoring the runs. Pressure and temperature sensors connected to a homemade LabView program record the thermodynamic path (Figure 1).

A nonpolarized Nd:YAG solid-state laser with a wavelength of 532 nm is used for the Raman analysis. After focusing onto a monochromator (Horiba JobinYvon HRi550, France) with a diffraction grating of 1,200 grooves/mm, the scattered light is detected with a charge-coupled device at 1,024 × 256 pixels, which is cooled to 203 K for thermal noise reduction. Fiber optics connect the spectrometer to a cryogenic probe with a focal lens of 23.6 mm (Microbeam S. A., Spain). The spectral resolution with a 200-μm-width slit produces results better than 5 cm^{-1}. Cyclohexane (PAI-ACS Panreac, Spain) is an appropriate standard pattern for the Raman shift wavenumber calibration in this study, since its Raman shift variations are lower than 1 cm^{-1} in the pressure-temperature range of this work (see the Supporting Information Figure S1; Pelletier, 1999; Qiao & Zheng, 2017).

The reagents used to prepare the samples are $MgSO_4{\cdot}7H_2O$ (≥99.5% purity, Sigma-Aldrich, USA), CO_2 gas (99.998% purity, Praxair, USA), and Milli-Q water. The high-pressure cell is completely filled with the aqueous solution, with the aim of recording the pressure changes due to volume variations during the stabilization/melting of the solid phases or gas dissolution/exsolution.

The general procedure employed to run the experiments is to add CO_2 to the aqueous sample while stirring at 3 MPa and 282 K for 1 week in order to ensure homogeneous saturation and then cool the solution to below 269 K, which is the eutectic temperature of the salty system, in order to reach complete crystallization. Once

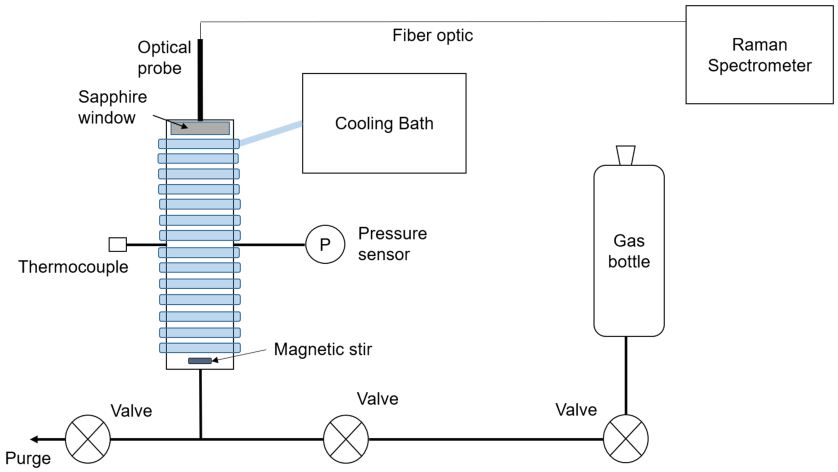


Figure 1. Diagram of the experimental setup. The high-pressure cell, equipped with pressure and temperature sensors and a sapphire window, is in a vertical position and is connected to a CO_2 tank with the temperature controlled by a cooling bath. The sapphire window allows for both spectroscopic and optical monitoring of the runs.

the formation of the solids is observed, the gas tank is closed, the stirring is stopped, and the system is kept at 267 K for 12 hr. The next step is to warm until the solids melt and, finally, recool to 267 K.

Variations of this general procedure are performed in some of the runs in order to check the effects of different paths (Table 1). We see that they cause deviations in the concentration ratio between the system compounds and in the changes in the physical state. Hence, it is necessary to keep in mind that gas solubility decreases with an increasing temperature and that the presence of salt hinders the dissolution of gases due to the attractive forces between the water molecules and the electrolytic salts dissolved in the aqueous solution (Bonales et al., 2013).

3. Results

We measured three types of data in the laboratory experiments: (i) thermodynamic, (ii) textural, and (iii) spectroscopic. The P-T-t and P/T paths were obtained for each experimental run. For the correct interpretation of the curves, we distinguish between the manually induced shifts (indicated by the protocol in Table 1) and the intrinsic changes in the system. Thus, in the P-T-t graphs, the P variations due to physical state transformations in the sample accompany T changes related to the endo/exothermic character of the reactions. Registered exothermic reactions generally correspond to crystallization processes. The P/T diagram is appropriate for following the phase changes. Pictures of features at the top of the chamber support the petrological evolution interpreted from the thermodynamic data. In all runs performed, a visually detected darkening of the aqueous solution always precedes the crystallization of solids. The Raman spectra characterize each observed phase formed during the evolution. We take the spectra at the center of the sapphire window unless otherwise indicated.

The combined study of these data taken from runs of both binary and ternary systems suggests several petrological findings:

3.1. The Evolution of the System Produces Mineral Diversity

When the fluid composed of H_2O and CO_2 is cooled to 267 K, it results in the crystallization of water ice I_h and CO_2-clathrates at the top of the high-pressure cell. The proportion between the two coexisting phases depends not only on the concentration of dissolved CO_2 but also on metastability effects, which are significant in the system, as we discuss later.

The P-T-t curve of Run 1 (Figure 2a) confirms that when the binary system solidifies via cooling, CO_2-clathrates and water ice coexist. Clathrates begin to form first, while water ice I_h stabilizes on two occasions as P jumps after 4 and 22 hr from the beginning of the run. In both cases, the system is in the stability field of water ice (Figure 2b). The Raman spectra allow for the identification of the characteristic signatures of

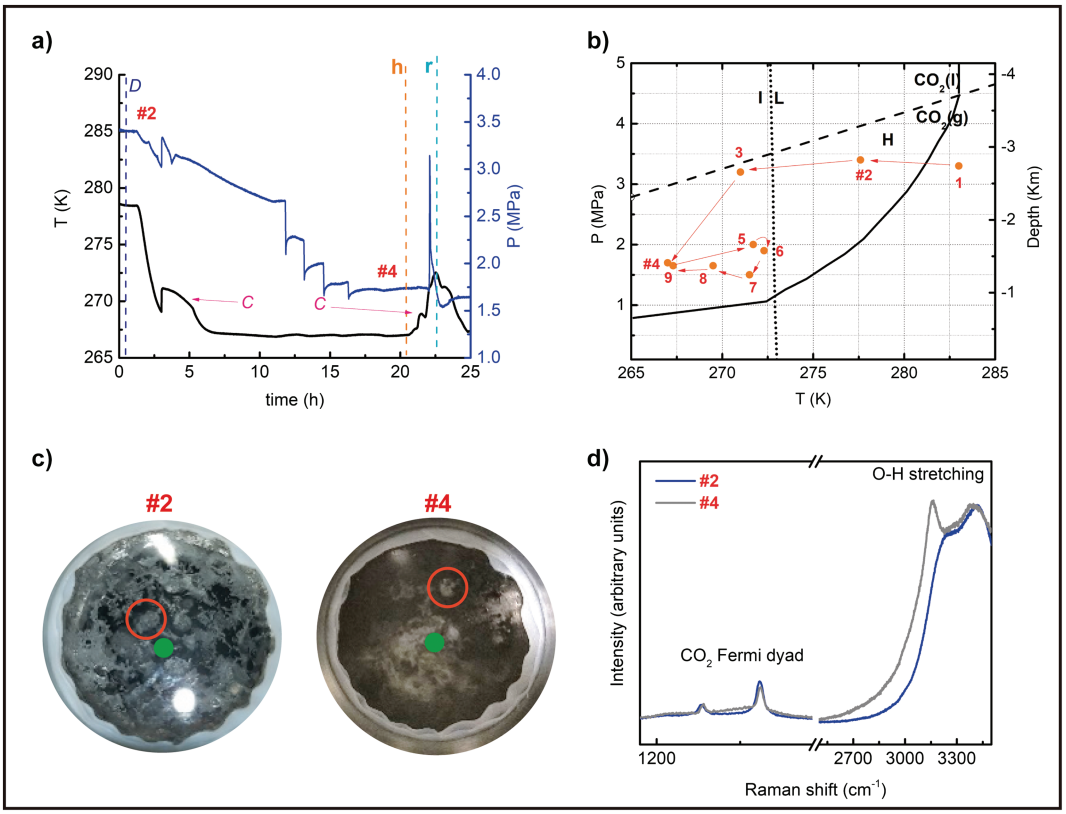


Figure 2. Run 1 data. (a) Pressure-temperature-time path, "D": solution darkening and subsequent crystal formation (stop gas filling and stirring), "C": crystallization events, "h": heating, "r": recooling; (b) pressure-temperature (P/T) path, "L": liquid water, "H": clathrate hydrate, "I": water ice I_h; (c) pictures at steps #2 and #4 of the run, indicated in the P/T path, where red circles mark an isolated crystal formed from aqueous solution (in #2) and a crystal trapped in the water ice matrix (in #4); (d) the Raman spectra taken at steps #2 and #4, where green points indicate the location of the laser spot.

the CO_2 molecule when it is inside the clathrate structure (the Fermi dyad peaks at 1,275 and 1,382 cm^{-1} move slightly to closer frequencies; see Muñoz-Iglesias et al., 2014, and references therein). Additionally, the relative intensity of the shoulder at 3,150 cm^{-1}, caused by the formation of multiple O–H bonds in both water ice I_h and clathrates, allows for control of the degree of crystallization of the total system during the run (Garcia-Baonza et al., 2012; Minceva-Sukarova et al., 1984). In the pictures, we observe that clathrate minerals appear isolated and are floating in the solution at the beginning of this run (Figure 2c, #2), and they remain trapped in the water ice matrix when the system crosses to the stability field of this phase (Figure 2c, #4).

Run 2 (Figure 3) exemplifies the dominance of CO_2-clathrate formation in the upper layers during cooling when the binary system is gas saturated. Clathrates nucleate and grow in association with protogenic bubble morphologies (Figure 3c). The Raman spectra confirm the main clathrate mineralogy of these textures (Figure 3d).

In Run 3 (Figure 4), the formation of CO_2-clathrates from the ternary system starts at the very beginning of the cooling immediately after a small amount of water ice forms. During the process, part of the salts precipitate as soon as the system reaches eutectic conditions, which is promoted by the higher concentration of sulfate due to water sequestering in the clathrate structure. Its main characteristic Raman signature in the aqueous state appears at 980 cm^{-1} and is caused by a symmetric stretch of the SO_4^{2-} molecule (see Figure S2). It must be mentioned that the decrease in the total volume after clathrate formation causes a loss in the sample Raman signal and an increase in the sapphire window contribution because of sample defocusing (see Figure S3; Kadleíková et al., 2001). This salting out effect occurs at different moments during the run. After 24 hr, the system is solid, showing equigranular crystals of clathrates at the top (Figure 4c) that have larger sizes than those formed in previous runs and display a phaneritic texture.

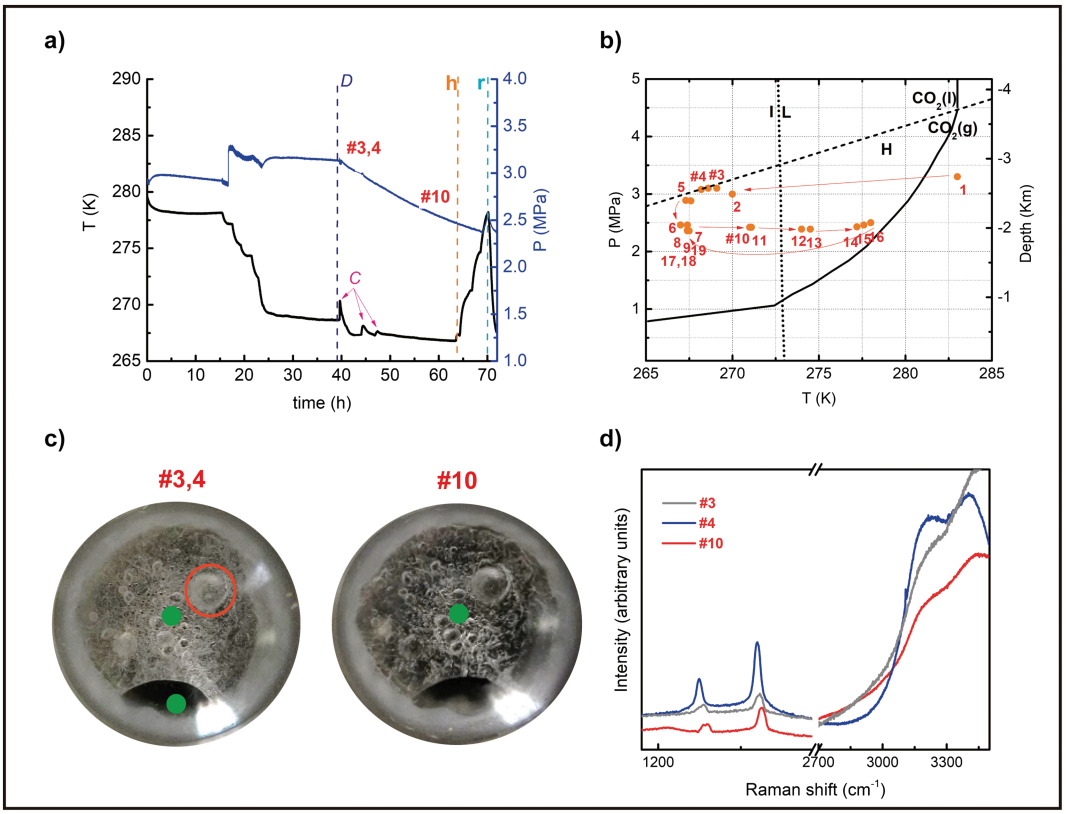


Figure 3. Run 2 data. (a) Pressure-temperature-time path, "D": solution darkening and subsequent crystal formation (stop gas filling and stirring), "C": crystallization events, "h": heating, "r": recooling; (b) pressure-temperature (P/T) path, "L": liquid water, "H": clathrate hydrate, "I": water ice I_h; (c) pictures at steps #3, #4, and #10 of the run, indicated in the P/T path, where the red circle marks a well-formed crystal immersed in a fine-grained matrix (in #3); at the bottom there is a metastable liquid drop (#4); after 24 hr of evolution, where the solids become more translucent (in #10); (d) Raman spectra taken at steps #3, #4, and #10, where green dots indicate the locations of the laser spots.

The cooling of the ternary system in Run 4 (Figure 5) also produces salt crystallization in addition to clathrate and water ice. However, here the substantial solvation of CO_2 fosters the initial concentration of the brine after 7 days of gas addition while stirring the system. Signatures in both parameters, P and T, in the range between 22 and 27 hr indicate this event. They correspond to the crystallization of meridianiite plus water ice when the peritectic and eutectic conditions are achieved (producing a change in the slope of the T curve and a peak, respectively). The crystallization occurs just before darkening of the solution, which follows a massive formation of clathrates (Figure 5c). The resulting texture is granular from the beginning (Figure 5c, #5), and crystal growth conforms to a botryoidal habit (Figure 5c, #6).

3.2. Metastability Induces Dramatic Changes Related to Crystal Growth Kinetics

The addition of $MgSO_4$ to the fluid increases the metastable characteristics of the system. During Run 5 (Figure 6), for instance, we observe no significant thermodynamic or textural changes until the heating step, despite maintaining the system in the stability field of clathrates + water and ice + meridianiite for 18 hr (Figures 6a and 6b). During the first cooling and stabilization to 273 K, some small pressure decreases occur after the injection of gas. However, no minerals are visually detected. Next, we cool the system to 267 K, resulting in no effect until 24 hr from the start, sustaining the solution in a liquid state. Then there is an exothermic peak correlated to the fluid enrichment in microparticles, which are potentially meridianiite and water ice. The Raman spectra show that CO_2 is in a solvated state during the experiment, and its

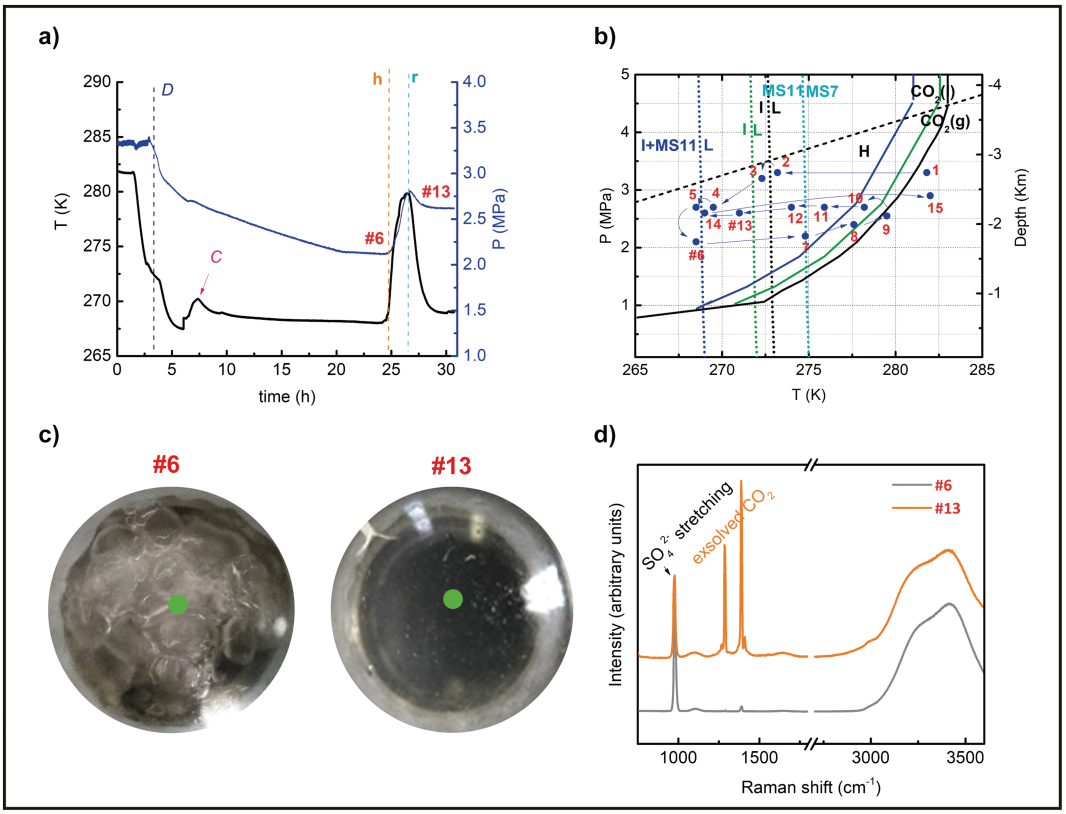


Figure 4. Run 3 data. (a) Pressure-temperature-time path, "D": solution darkening and subsequent crystal formation (stop gas filling and stirring), "C": crystallization events, "h": heating, "r": recooling; (b) pressure-temperature (P/T) path, "L": liquid water, "H": clathrate hydrate, "I": water ice I_h; (c) pictures at steps #6 (crystals with phaneritic structure) and #13 (CO_2 gas exsolved after the heating) of the run, indicated on the P/T path; (d) Raman spectra taken at steps #6 and #13, where green points indicate the locations of the laser spots.

concentration increases due to the gas salting out, which is promoted after salts and water ice stabilization (Figure 6d).

Metastability also characterizes Run 6 (Figure 7). The liquid state prevails throughout most of the run. Crystal growth occurs only in the interval between 23 and 35 hr during the first cooling. The shift in temperature after the gas injection at 25 hr indicates that water ice and meridianiite are the principal minerals formed. We visually detect the formation of a large crystal floating deep in the solution (the crystal can be observed only when the solution is illuminated with the green laser beam of the Raman spectrometer, Figure 7c, #5, #6) and some smaller crystals covering the chamber walls. Then, a second exothermic peak marks the appearance of a metastable brine pocket adhered to the wall. The Raman spectra reveal that this droplet is very rich in $MgSO_4$ at 21 wt% (Figure 7d).

3.3. Chemical Differentiation is Favored

Generally, the final trend after cooling the ternary system is the presence of clathrates and water ice I_h at the top and sulfate hydrates at the bottom of the high-pressure cell. However, small procedural modifications applied to each run (Table 1) result in important variations in the system evolution, as previously observed in Runs 3 and 4.

The variation in the sulfate concentration in the top layers of the solution can be quantified from the Raman spectra (Figure 8; the calibration curve previously made for this analysis is shown in Figure S2; Walrafen et al., 1986; Rudolph et al., 2003). Two combined factors affect the brine concentration during the experiments. On one hand, both water ice I_h and clathrate formation produce increases in the sulfate content of the remaining aqueous solution due to the salting-out effect, since salts are not part of the crystal

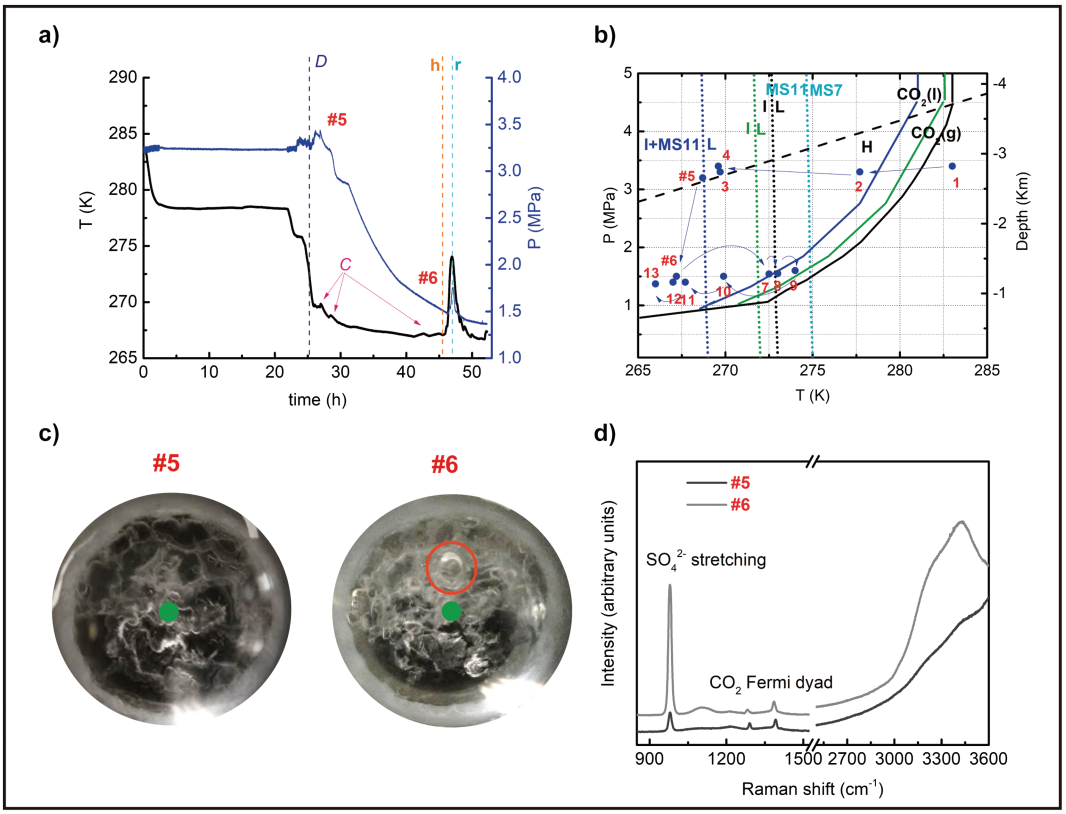


Figure 5. Run 4 data. (a) Pressure-temperature-time path, "D": solution darkening and subsequent crystal formation (stop gas filling and stirring), "C": crystallization events, "h": heating, "r": recooling; (b) pressure-temperature (P/T) path, "L": liquid water, "H": clathrate hydrate, "I": water ice I_h; (c) pictures at steps #5 (crystals with granular structure) and #6 (red circle denotes a botryoidal crystal) of the run, indicated in the P/T path; (d) Raman spectra taken at steps #5 and #6, where green points indicate the locations of the laser spots.

structures of these solids (Méndez et al., 2017). On the other hand, the consequent precipitation of sulfate hydrates promoted by both cooling and salt oversaturation results in a subsequent decrease in the aqueous sulfate concentration.

3.4. Local Heat Pulses and Recrystallization Produce Further Evolution

When we heat and recool the system for a second time, the response is different among the experiments depending on the protocol used and the derived conditions of the previous step. While the recrystallization of the binary system runs results in the stabilization of habits similar to those in the first cooling, particular processes occur in the ternary systems. In Run 1, solids remain because the stability of ice is not overtaken. However, in Run 2, the water ice matrix melts and recrystallizes. The retention of the low-pressure values in both runs indicates that most of the clathrates are not lost.

In Run 4, the fractional crystallization of sulfates decreases the salt concentration, producing a shift back to higher temperatures on the stability line of clathrates. This situation prevents clathrate dissociation, even if we force their destruction by approaching the curve temperatures. In contrast, we heat Run 3 to higher temperatures. Hence, clathrates partially dissociate, and the Raman measurements detect the CO_2 gas with signals appearing at 1,286 and 1,389 cm^{-1} with the additional two small vibrations known as hot bands, which are caused by minor transitions (at 1,265 and 1,410 cm^{-1}; Sathyanarayana, 2004; Sloan & Koh, 2007). The strong CO_2 exsolution results in a salting-in effect. The later second cooling does not promote the redissolution of the gas until the salts are removed (Figure 4).

Because no significant clathrates form in Runs 5 and 6, the heat pulses in both runs result in an isobaric effect. We visually detect the redissolution of the brine pockets in Run 6 while heating (see Figure S4).

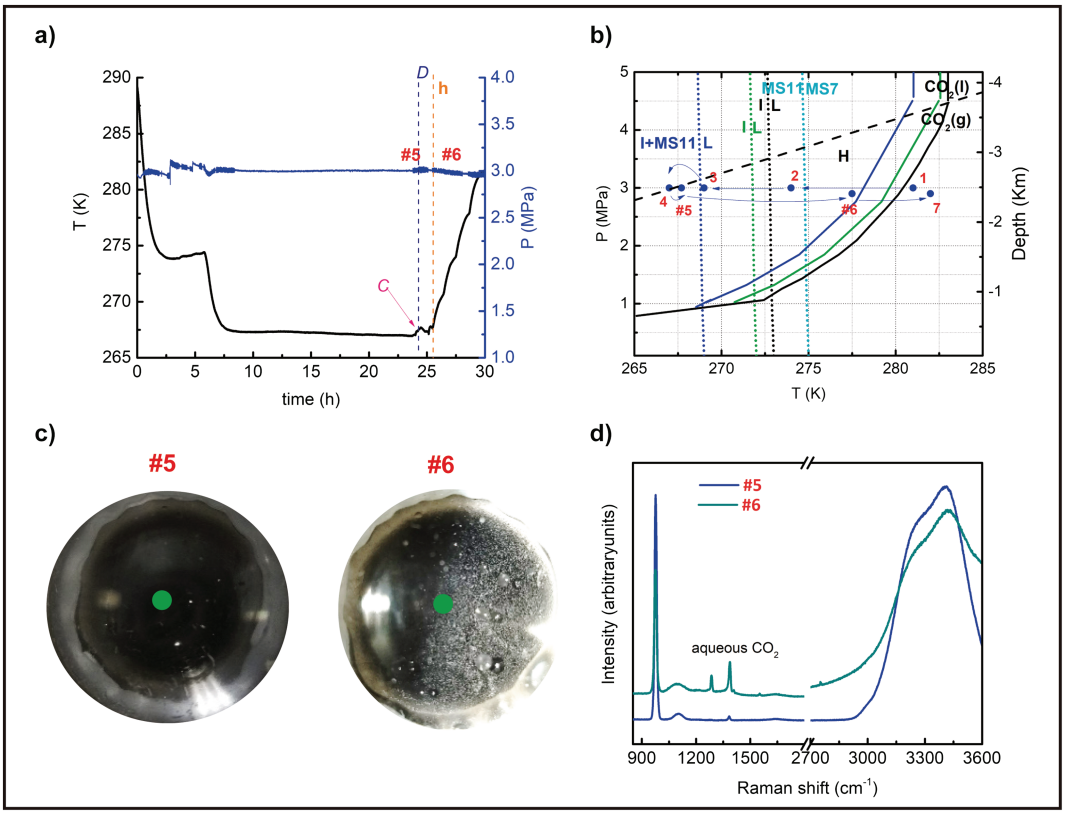


Figure 6. Run 5 data. (a) Pressure-temperature-time path, "D": solution darkening and subsequent crystal formation (stop gas filling and stirring), "C": crystallization events, "h": heating; (b) pressure-temperature (P/T) path, "L": liquid water, "H": clathrate hydrate, "I": water ice I_h; (c) pictures at steps #5 (just before nucleation) and #6 (crystal nuclei immersed in aqueous solution) of the run, indicated on the P/T path; (d) the Raman spectra taken at steps #5 and #6, where green points indicate the locations of the laser spots.

4. Discussion

4.1. Planetary Evolution of Fluids at Low Temperature

All runs are performed mostly below 4 MPa (except in the heating of Run 6, where the system reaches 5.6 MPa), which represents the top 3 km beneath the surface, considering a crust mainly composed of pure water ice (Bonales et al., 2013).

The experimental results provide arguments for discussing the geologic activity of Europa with respect to the cryomagmatism and their possible connection with the surface features (Figure 9). As we have seen, there are four important findings: (1) The evolution of the fluid produces mineral diversity; (2) metastability induces dramatic changes in the crystal growth kinetics; (3) chemical differentiation is favored; and (4) secondary heat pulses and recrystallization produce further evolution. The situations that have been modeled in this work include (a) the ascent, emplacement, and cooling of a cryomagma in the upper crust; and (b) the secondary evolution related to reheating of the system by the intrusion of a second pulse of additional heating near the surface (e.g., Quick & Marsh, 2016; Han & Showman, 2010; Figueredo et al., 2002; Sotin et al., 2002; Rathbun et al., 1998). This reheating could lead to mineral destabilization, incongruent melting (incongruent cryomagmatism), and the formation of new mineral phases during secondary crystallization.

Although we have represented the cryomagmatic bodies with a diapiric morphology in Figure 9, our model tests the roles that composition and thermal events play in the evolution of cryomagmas. These roles are independent of the emplacement mechanism or the shape of the emplaced body (diapirs, dikes, sills, laccoliths, etc.). Thus, petrology results complement those of previous works focused on the emplacement mechanisms (e.g., sills; Michaut & Manga, 2014; Craft et al., 2016) and suggest that both the composition and emplacement mechanism play important roles in the ascent of cryomagmas and the final morphology of associated surface features.

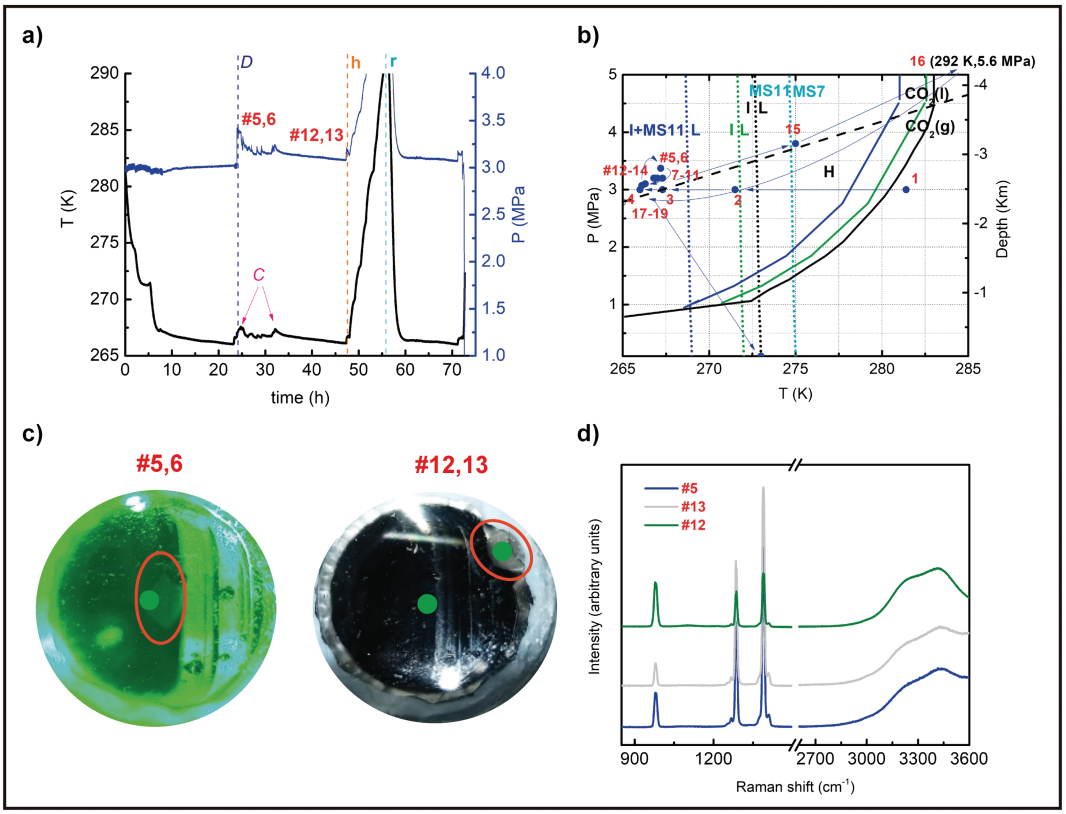


Figure 7. Run 6 data. (a) Pressure-temperature-time path, "D": solution darkening and subsequent crystal formation (stop gas filling and stirring), "C": crystallization events, "h": heating, "r": recooling; (b) pressure-temperature (P/T) path, "L": liquid water, "H": clathrate hydrate, "I": water ice I_h; (c) pictures at steps #5, #6 (CO_2-clathrate layers and an isolated crystal located at depth marked by a red circle), #12 (salty drop marked by a red circle), and #13 (dark aqueous solution) of the run, indicated in the P/T path; (d) the Raman spectra taken at steps #6, #12, and #13, where green dots indicate the locations of the laser spots.

Many of the geological features that are discussed (pits, uplifts, spots, and microchaos) appear to be spatially related or even clustered (e.g., pits; Pappalardo et al., 1998; Spaun et al., 2001; Culha & Manga, 2016). These spatial and temporal relationships indicate that the processes responsible for the different structures can interact in space and time, producing local reheating and modification of the previous events.

The ascent, cooling, and crystallization of cryomagmas involve different endo/exothermic chemical reactions that can result in associated phase changes. These processes, together with the presence and behavior of volatiles in the cryomagma, produce variations in the volume of the diapir and, consequently, in the local pressure of its surroundings. The overpressures related to volume changes during the partial freezing of the emplaced bodies can be the driver for structures found on the surface if emplacement takes place near the surface (Craft et al., 2016; Fagents, 2003; Manga & Wang, 2007; Pappalardo et al., 1999). The volume changes observed in our experiments are related to the different mineral phases formed in the studied systems (Muñoz-Iglesias et al., 2014). Thus, when water ice I_h crystallizes, the volume increases, and the diapir subsequently expands. On the other hand, the stabilization of CO_2 clathrates causes a contraction of the diapir due to gas trapping. The formation of sulfate minerals implies a large variety of volume changes related to the type of sulfate formed (they form with different levels of hydration), which depends on the salt content of the initial aqueous solution and on the P-T conditions when precipitation occurs (Genceli et al., 2007; Hogenboom et al., 1995; Kargel, 1991). In the cryomagmas considered for this work (H_2O–CO_2 and H_2O–CO_2–$MgSO_4$; 15-wt% $MgSO_4$ aqueous solution), the global changes observed are contraction during cooling and expansion during heating. Reheating the cryomagma would cause mineral dissociation, incongruent melting processes, and even volatile exsolution if the volatiles are present, and the temperature reach is sufficiently high. The presence of discontinuities in the crust would result in a release to the exosphere of volatiles that come from processes driving exsolution.

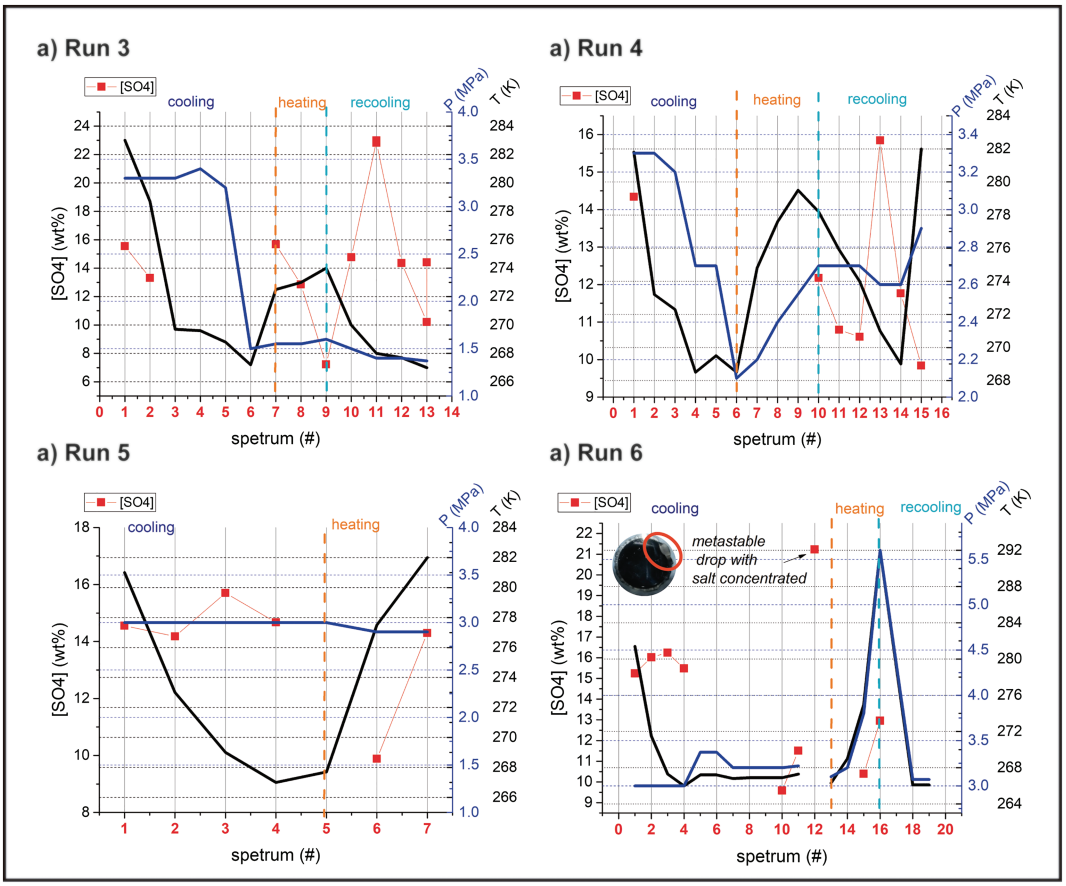


Figure 8. Changes in the sulfate concentration during runs of the ternary system H_2O–CO_2–$MgSO_4$, measured from the Raman spectra taken at the center of the window, except for #12 of Run 6, which corresponds with the sulfate content of a salt-rich metastable drop indicated in the picture.

Chemical differentiation observed in experiments where $MgSO_4$ is added to the cryomagma causes stratification in the high-pressure cell. In Runs 3 and 4, the hydrated sulfate crystals sink to the bottom due to their higher density, with the less dense phases of the CO_2-clathrates and water ice I_h remaining on top. This process of mineral separation in the cryomagmas suggests that the upper levels of the diapir (or even the entire crust), where these processes take place, would be enriched in H_2O and volatiles with respect to the lower levels, which would be richer in sulfate hydrates.

The salting-out effects of both gases and salts also play important roles in cryomagmatism. This mechanism, together with the high metastabilities found at low temperatures, causes the existence of more mineral or volatile phases at certain P-T conditions than previously expected. The stability shifting in favor of one final phase or another will also have consequences in the system's physical properties that affect the crust.

Volatiles in aqueous solutions can explain the ascent of cryomagmas as volatiles increase buoyancy (Crawford & Stevenson, 1988; Fagents et al., 2000; Muñoz-Iglesias et al., 2014). These volatiles stabilize as clathrates during the cooling phase of the cryomagma, but if a reheating phase takes place, they exsolve again, which could be important for the secondary evolution of the cryomagmatic body (Figure 9).

The high probability of the occurrence of other impurities such as chlorides and sulfuric acid in the crust, most of them with lower melting points than sulfates, must be considered. The higher solubility of these other types of impurities in water (i.e., their eutectic compositions lie at higher concentrations) promotes an increase in the ion-water interactions and a consequent decrease in the CO_2 or other solubilized hydrate guest due to the gas salting-out effect. These processes cause a decrease in the melting equilibrium curves of both the clathrates and water ice. Bakker et al. (1996) theoretically predicted these boundary changes for CO_2 clathrates in NaCl, KCl, and $CaCl_2$ aqueous solutions at temperatures down

to 253 K and pressures up to 200 MPa. Prieto-Ballesteros et al. (2005) estimated clathrate inhibition in the presence of magnesium sulfate aqueous solutions with different concentrations at 5, 10, and 17 wt%. In some cases, it is observed that a decrease in the clathrate melting temperature is parallel to the corresponding water ice. However, in other cases, although still following a similar trend, the inhibition effect is smaller for clathrates. For instance, an NaCl eutectic aqueous solution (i.e., 21 wt%) leads CO_2-clathrates to melt at 260 K at 1 MPa and water ice at 252 K, while these events in pure water occur at 277 and 273 K, respectively. Thus, the CO_2-clathrate equilibrium curve decreases by 17 K while water ice decreases by 21 K, increasing the gap with the salt concentration (Bakker et al., 1996). Assessing the CO_2 solubility in these aqueous solutions at low temperatures (Bonales et al., 2013; Markham & Kobe, 1941; Portier & Rochelle, 2005) will be very interesting, together with the variations in the clathrate equilibrium curves, using experimental procedures similar to the ones employed in this study. It will also be valuable to experimentally determine the equilibrium locations regarding the pressure and the differences between the thicknesses of the different layers of water ice, clathrates, and salts/sulfuric acid hydrates. From experimental simulations, it will be possible to elucidate whether systems with lower eutectics allow for the formation of thicker clathrate layers or conversely the stabilization of larger aqueous diapirs. Additionally, their evolution over larger timescales will be assessed by incorporating the new data into theoretical models. The calculations mentioned here will be the focus of future work.

4.2. Cryomagmatic Features on Europa and Their Relation to the Experiments

Numerous cryomagmatic features pepper the surface of Europa. Pits, spots, uplifts, and small patches of chaotic terrain (or microchaos) are thought to be the surface expressions of processes that take place in the ice shell or the underlying ocean. Proposed models for their formation include rising diapirs or related intrusive structures such as sills (Craft et al., 2016; Greenberg et al., 2003; Michaut & Manga, 2014; Pappalardo & Barr, 2004). Their similar sizes and locations could indicate that they share a common origin and are different surface manifestations or evolutionary phases of the same process (Greenberg, 1999; Pappalardo et al., 1998). Our observations are applicable for explaining the petrological and structural characteristics of the materials associated with endogenous features.

4.2.1. Structures Derived From Cryoplutonic Diapirs: Uplifts, Pits, Spots and Microchaos

Uplifted areas are often observed on Europa images (Greenberg et al., 2003). Although these features are designated as domes in other works (e.g., Pappalardo et al., 1998), in this work we use the general term uplifts, and we reserve the term dome for those structures interpreted as extrusive features (e.g., Fagents, 2003; Quick et al., 2017). Uplifts are present with different morphologies and sizes (circular, irregular, or polygonal), and only on rare occasions do they disrupt the surface (<3%; Greenberg et al., 2003). These uplifts would be analogous to the Type 2 domes of Pappalardo and Barr (2004) that occasionally also appear disrupted (e.g., Figure 1c in Pappalardo & Barr, 2004). Unlike other features of the same size, they are rarely associated with dark materials (Greenberg et al., 2003), meaning waterless ice compounds such as hydrated sulfates, hydrated sulfuric acid, and chlorides (Dalton et al., 2005; Dalton et al., 2013; Hand & Carlson, 2015; McCord et al., 1998; McCord et al., 1999; Orlando et al., 2005).

Their morphology and lack of surface disruption in most cases (Pappalardo & Barr, 2004) suggest that their formation is related to limited upwarping of the surface in response to the push-up force produced by a rising diapir or by volume expansion in response to phase changes in the emplaced diapir (u in Figure 10a). Uplifts where disruption cannot be observed are analogous to the surface expression of laccoliths on Earth (Pappalardo & Barr, 2004), where minor deformations on the surface can be found in the form of monoclinal folds. In uplifts that are fractured but lack associated dark materials, fracturing could be accompanied by cryovolcanism of relatively "clean" water ice. In any case, freezing of water ice and its associated increase in volume as a driver for the upwarping of the surface must be involved in the uplift formation. We have reproduced this process of uplift driven by volume changes in Run 1 (Figure 9), where the formation of water ice I_h and the associated expansion in the upper part of a diapir emplaced in a similar lithology close to the surface could produce the push-up force responsible to uplift the surface without breaking it. The exothermic characteristic of water crystallization may favor deformation without rupture. The size and magnitude of the uplift would then be related to the size of the diapir and/or the depth of the emplacement (i.e., emplacement closer to the surface would favor uplift or even lead to disruption in those cases when this occurs). This disruption could also take place if secondary heating takes place (Figure 9), but in all these cases only water ice compositions would be involved.

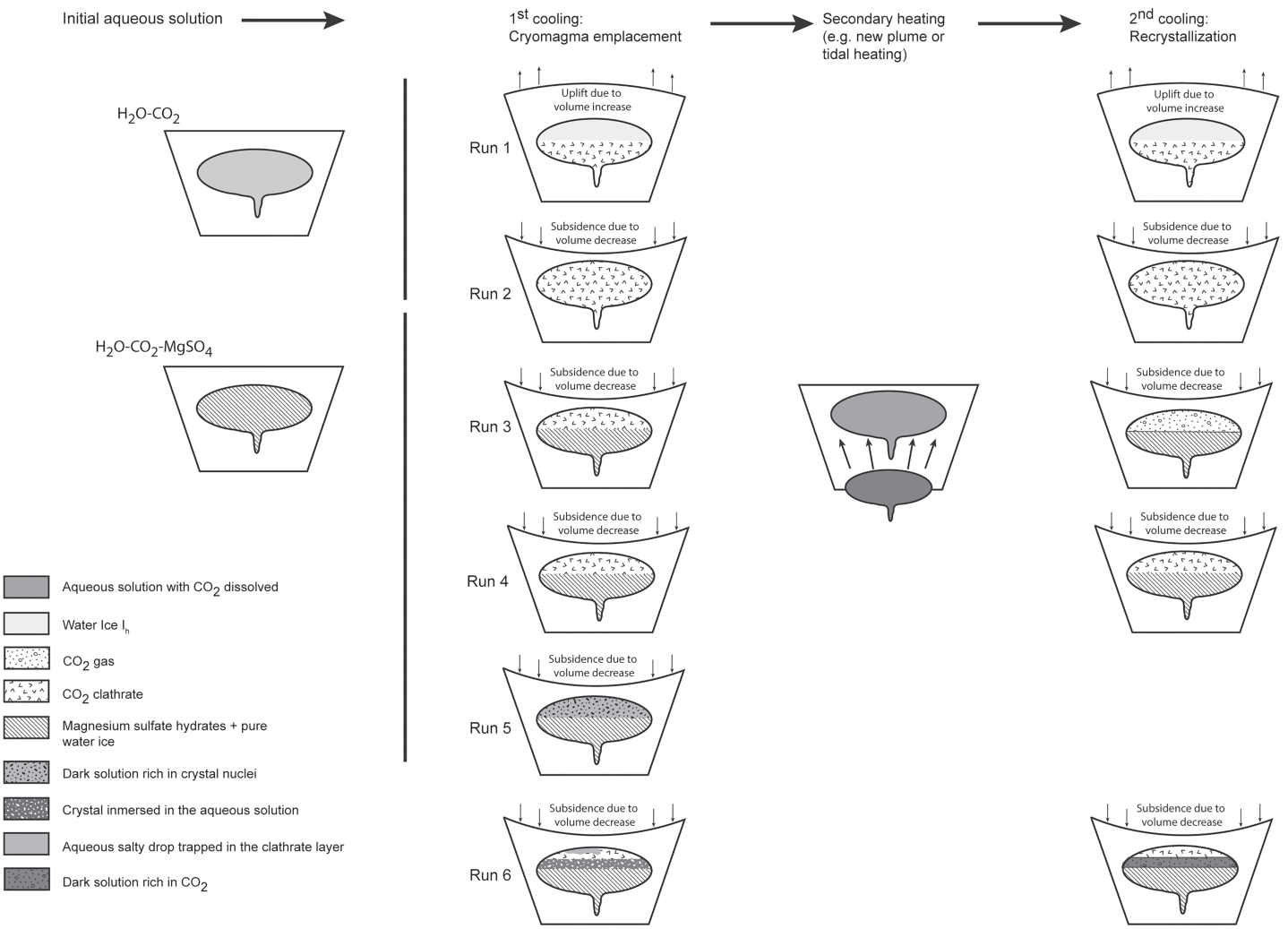


Figure 9. Schematic description of the physico-chemical changes observed in the cryomagma during the runs. See the text for a comparison with structures found on the surface.

Pits are common surface features on Europa, but their origin is not yet understood. They are negative relief features (200–300 m in depth; Shenk & McKinnon, 2001, Greenberg et al., 2003) that, as in the case of uplifts, do not appear to disrupt the surface (p, Figures 10b and 10c). According to Culha and Manga (2016), pits are clustered in certain regions, whereas uplifts and chaos are more uniformly distributed, suggesting that local properties of the ice shell control the formation of pits (Michaut & Manga, 2014).

Pits can be formed due to local heating and melting of water ice in the subsurface, which produces a decrease in the volume below the surface, resulting in subsidence (Culha & Manga, 2016; Greenberg et al., 2003). In this scenario, pits could be genetically related to chaos, with pits a preceding stage before chaos formation or the result of aborted or incomplete melt-through. Recent models propose that pits are the result of the emplacement of sills under the surface (Culha & Manga, 2016; Michaut & Manga, 2014) and that pits evolve into domes, dome/chaos, and chaos depending on the volume of the liquid body and the crustal properties.

Spots are also smooth, concave, or depressed structures. Unlike pits, they obscure preexisting terrain (Carr et al., 1998; Pappalardo et al., 1998; Fagents et al., 2000; Fagents, 2003; Miyamoto et al., 2005). They are scarce and, when present, have sizes similar to those of pits (Culha & Manga, 2016), suggesting that the two features are genetically related (i.e., spots are pits with their interiors filled by materials of low albedo that cover preexisting structures; s in Figure 10d). The low albedo of spots can be the result of differences in the grain size or in composition (e.g., hydrated salts; McCord et al., 1999).

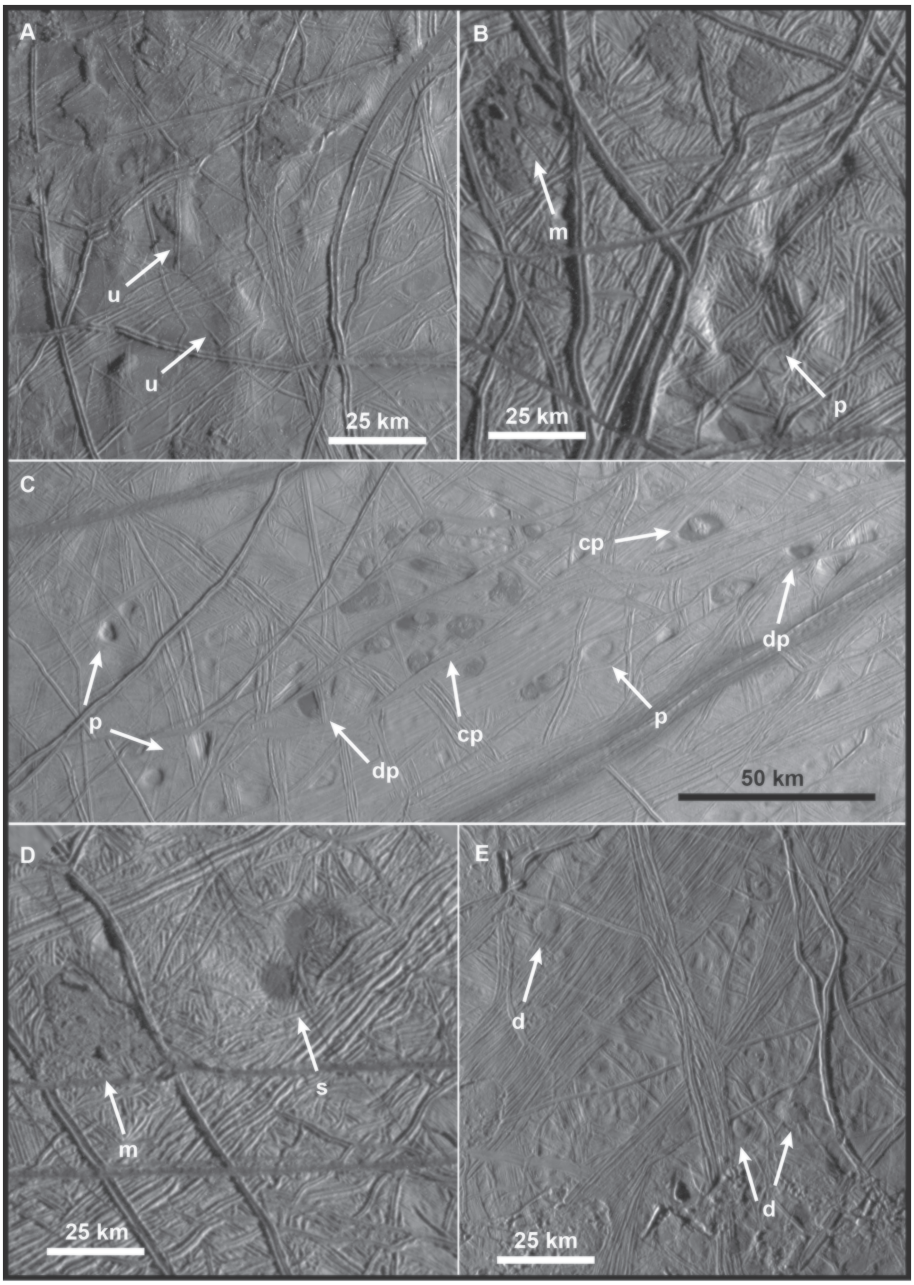


Figure 10. Geological features formed in response to the emplacement of cryomagmatic bodies beneath the surface. All images are illuminated from the southwest (NASA/JPL/UA/Jason Perry). (a) Examples of uplifts without surface disruption (u). (b) Examples of pits (p) and microchaos (m). Note the collapse without surface disruption of pits. (c) Examples of clustered pits with different characteristics: pits without surface disruption (p), pits with dark floors (dp), pits with surface disruption, and small chaos inside (cp). (d) Examples of spots (s) and microchaos (m). Note the dark floors in that spots that indicate the filling of depressions by low-albedo materials. (e) Examples of extrusive domes (d).

Small chaos regions or microchaos are dark features, where the surface is disrupted and broken into blocks (e.g., m in Figures 10b and 10d). Their topography is more complex than those of uplifts and pits, with some presenting uplifted morphologies, while others appear depressed and with some described as "moats" surrounding a central chaos area (Greenberg et al., 2003). Recrystallization is also associated with a decrease in volume and could be responsible for the formation of more complex topographies (e.g., moats surrounding central elevations; cp in Figure 10c). This topographic complexity results in

some classification problems. Recent works have described a new category named dome/chaos (e.g., Culha & Manga, 2016), and some of the initially defined spots are microchaos regions when observed at higher resolutions. These classification problems could be addressed with the future acquisition of higher resolution images and topographic data.

The presence of liquid water at or near the surface seems to be necessary to explain the small chaos regions (the same applies to large chaos regions; Schmidt et al., 2011; Carr et al., 1998), although some of the characteristics of small chaos suggest the presence of compositions other than pure ice (e.g., low albedo features). The formation of microchaos requires melt-through or near-surface melting, a process that is not easy to achieve from an energy point of view if only heat flow transmitted from ocean plumes is considered (Goodman et al., 2004). The volatiles and hydrated salts as modeled in our experiments can play important roles in the formation of small chaos regions. Volatiles would then be responsible for enhancing buoyancy and breaking the surface while salts promote the required melting due to their thermal properties.

The pits, spots, and microchaos can be formed in the situations reproduced in Runs 2–6 (Figure 9), which are associated with a decrease in the volume that is expected in these situations. The simplest morphology, pits with undisrupted surfaces (p in Figure 10b), can be explained by contraction related to the cooling of a diapir near the surface. The formation of CO_2-clathrates (Run 2) and CO_2-clathrates and magnesium sulfate hydrates (Runs 3 and 4) would have an associated decrease in total volume, which could explain the observed surface subsidence. The magnitude of the subsidence would be, as in the case of uplifts, related to the size and depth of the emplacement of the diapir, but in this case the amount of volatiles present in the cryomagma could also play a major role in the final configuration of the surface structure. In this situation, compositional differentiation could have segregated clean gassy fluids; therefore, no material reaches the surface and fills the formed depression (i.e., undisrupted surface). In circumstances where a secondary heating event takes place without gas release, there would be a local variation in volume associated with the new melting (increase in volume), followed by a new recrystallization event in the second cooling. The presence of different emplacement events and their associated reactivation phases could be responsible for the presence of overlapping pits and spots (e.g., p in Figures 10b and 10d). Secondary heating would also produce a new volatile exsolution event (i.e., clathrate destabilization) that increases the buoyancy of the diapirs and helps fractures propagate to the surface (Crawford & Stevenson, 1988; Fagents, 2003). As experiments show in the multicomponent system, salts concentrate when clathrates forms, sometimes comprising the brine pockets. They will crystallize when mixed with the ices (see Figure 7d, Run 6) or over them if their permeability does not permit the downward percolation (Schmidt et al., 2011). If magnesium sulfate hydrates reach the surface, they fill the depressions and could account for the formation of some spots or pits with dark floors and reddish materials that disrupt the previous surface (dp in Figure 10c and s in Figure 10d). The metastability property of these systems permits supercooling, so fluids might even be transported out of the thermal equilibria. The formation of microchaos occurs when the disruption of the surface is complete. As in previous cases, this could be related to the magnitude of the secondary thermal events, and/or the depth of emplacement in the first phase, and to the amount of volatiles involved and the magnitude of the secondary heating.

Recrystallization, if clathrates are present, would also be associated with a decrease in volume in the subsurface and could be responsible for the formation of more complex topographies described in small chaos regions (e.g., moats).

4.2.2. Cryovolcanism: Domes and Geysers

Although extensive flooding is not resurfacing Europa, localized cryovolcanism must be important in the geologic evolution of the icy satellite (Fagents, 2003; Quick et al., 2017). For cryovolcanic events to occur, it is necessary to have a pressure-driven ascent through fractures that connect the diapir with the surface and/or the presence of volatiles that increase the buoyancy of the cryomagma (Crawford & Stevenson, 1988; Fagents et al., 2000; Muñoz-Iglesias et al., 2014). In our experiments, the emplaced diapir is pressurized in response to the lithostatic pressure of the surrounding icy crust. The materials of the diapir could actively reach the surface if they ascend through fractures that would open in response to this excess pressure and if the diapir is near the surface (Fagents, 2003; Quick & Marsh, 2016). Alternatively, large fractures formed in response to tidal stresses could reach higher depths and connect the diapir with the surface in a more sudden or catastrophic way. Here, we consider two manifestations of such cryovolcanism: extrusive domes and eruptive geysers.

Several domes disrupt and overlap surface features, which have thus been interpreted as having a volcanic origin (Fagents, 2003; Pappalardo et al., 1998; Quick et al., 2017). These domes are composed of materials that are texturally different than preexisting terrain (Figure 10e), analogous to Type 1 domes of Pappalardo and Barr (2004). On Europa, these extrusive domes could be formed by (a) low-viscosity water cryolavas that undergo rapid cooling (Quick et al., 2017), (b) a mixture of liquid water and ice with a slushy texture (Fagents, 2003), and (c) relatively viscous solutions composed of water and non-ice contaminants, such as sulfate salt hydrates (Fagents, 2003; Hogenboom et al., 1995; Kargel, 1991; Muñoz-Iglesias et al., 2013, 2014; Quick et al., 2017). According to these considerations, the compositions used in our experimental runs could produce extrusive domes, provided that the cryomagmas reach the surface. In the systems considered in Runs 3 and 4, the presence of gas hydrates and sulfate salts would be important for providing the volatiles for the cryomagma to reach the surface and for increasing the viscosity of the cryomagma, respectively. In these situations, if the cryomagmas that ascend through fractures reach the surface, the volatiles would be liberated, and a viscous supercooled solution formed by the water and magnesium sulfate would be extruded. In the case of Run 5, the dark solution rich in crystal nuclei is a candidate to produce an extrusive dome if the high-viscosity slurry is connected to the surface through a fracture. The first of the possibilities, low-viscosity water cryolavas that undergo rapid cooling (Quick et al., 2017), could correspond to compositions considered in Runs 1 and 2, where water ice would reach the surface. In all these situations, the ascent of cryomagmatic solutions in fractures is pressure-driven by the volatiles present in the cryomagma. The ascent of high-density fluids (i.e., fluids that are usually negatively buoyant with respect to the surrounding ice) through the upper crust would be gradual and might allow the cryomagma to evolve, as in the processes modeled in the experimental procedures.

The recent detection of water plumes at the south hemisphere of Europa suggests the existence of active explosive cryovolcanism (Roth et al., 2014; Sparks et al., 2016; Sparks et al., 2017). Several mechanisms can form water plumes, such as the explosive release of volatile compounds exsolved from the fluid as the confining pressure is removed (Bonales et al., 2013; Crawford & Stevenson, 1988; Fagents et al., 2000; Pappalardo et al., 1999), pressurization and fracturing due to volume changes produced in response to the freezing of water in a closed diapir (Fagents et al., 2000; Pappalardo et al., 1999; Schmidt et al., 2011; Walker & Schmidt, 2015), and vapor release due to boiling associated with the effusion of liquid cryolavas (Fagents, 2003; Quick et al., 2017), although plumes caused by this last mechanism might be much smaller than those observed by Roth et al. (2014) and Sparks et al. (2016, 2017). All of our runs where volatiles accumulate in the upper part of the diapir could produce explosive volcanism if they are suddenly connected to the surface through a fracturing event (Runs 1–4), especially in the case of secondary heating in Run 3, where CO_2 gas would accumulate in the upper part of the cryomagmatic diapir (Figure 9). Further work would require knowing the precise location of these explosive events and studying the sites where this volcanic activity takes place in detail in order to ascertain whether effusive volcanism is also associated with the formation of the explosive plume.

5. Conclusions

The results of the experimental petrology at a low temperature help in understanding the evolution of Europa's crust. We measured the thermodynamic and petrographic characteristics of selected chemical systems, including the fabric, composition, and phase changes, during different simulated P-T-t paths. We conclude that, depending on the initial composition and the P-T-t path, different events take place in the system. With our experiments, we showed that all the processes studied in this paper generate incongruent melting, volume changes, and local overpressure associated with phase changes, discontinuities in solids, or bubble-rich fluids. Our observations can explain some of Europa's features that are interpreted as cryomagmatic in origin, such as pits, domes, or plumes.

Acknowledgments
The authors would like to thank the reviewers for their careful and constructive comments that have helped to improve this work. This work was supported by the Spanish MINECO projects ESP2014-55811-C2-1-P and ESP2017-89053-C2-1-P and the AEI project MDM-2017-0737 Unidad de Excelencia "María de Maeztu." The authors comply with AGU's data policy. Data are publicly available (DOI: 10.5281/zenodo.2620517).

References

Anderson, J. D. (1998). Europa's Differentiated Internal Structure: Inferences from Four Galileo Encounters. *Science*, *281*(5385), 2019–2022. https://doi.org/10.1126/science.281.5385.2019

Arnold, H., Liuzzo, L., & Simon, S. (2019). Magnetic Signatures of a Plume at Europa During the Galileo E26 Flyby. *Geophysical Research Letters*, *46*(3), 1149–1157. https://doi.org/10.1029/2018GL081544

Bakker, R. J., Dubessy, J., & Cathelineau, M. (1996). Improvements in clathrate modelling: I. The H2O-CO2 system with various salts. *Geochimica et Cosmochimica Acta*, *60*(10), 1657–1681. https://doi.org/10.1016/0016-7037(96)00032-4

Bierhaus, E. B., Zahnle, K., & Chapman, C. R. (2009). Europa's crater distributions and surface ages. In R. T. Pappalardo, W. B. McKinnon, & K. Khurana (Eds.), *Europa*, (pp. 161–180). Tucson, AZ: University of Arizona Press.

Bonales, L. J., Muñoz-Iglesias, V., & Prieto-Ballesteros, O. (2013). Raman spectroscopy as a tool to study the solubility of CO2 in magnesium sulphate brines: Application to the fluids of Europa's cryomagmatic reservoirs. *European Journal of Mineralogy*, *25*(5), 735–743. https://doi.org/10.1127/0935-1221/2013/0025-2312

Brown, M., & Hand, K. (2013). Salts and radiation products on the surface of Europa. *The Astronomical Journal*, *145*(4), 110. https://doi.org/10.1088/0004-6256/145/4/110

Carlson, R., Smythe, W., Baines, K., Barbinis, E., Becker, K., Burns, R., et al. (1996). Near-infrared spectroscopy and spectral mapping of Jupiter and the Galilean satellites: Results from Galileo's initial orbit. *Science*, *274*(5286), 385–388. https://doi.org/10.1126/science.274.5286.385

Carr, M. H., Belton, M. J. S., Chapman, C. R., Davies, M. E., Geissler, P., Greenberg, R., et al. (1998). Evidence for a subsurface ocean on Europa. *Nature*, *391*(6665), 363–365. https://doi.org/10.1038/34857

Collins, G. C., Head, J. W., Pappalardo, R. T., & Spaun, N. A. (2000). Evaluation of models for the formation of chaotic terrain on Europa. *Journal of Geophysical Research, Planets*, *105*(E1), 1709–1716. https://doi.org/10.1029/1999JE001143

Craft, K. L., Patterson, G. W., Lowell, R. P., & Germanovich, L. (2016). Fracturing and flow: Investigations on the formation of shallow water sills on Europa. *Icarus*, *274*, 297–313. https://doi.org/10.1016/j.icarus.2016.01.023

Crawford, G. D., & Stevenson, D. J. (1988). Gas-driven water volcanism and the resurfacing of Europa. *Icarus*, *73*(1), 66–79. https://doi.org/10.1016/0019-1035(88)90085-1

Culha, C., & Manga, M. (2016). Geometry and spatial distribution of lenticulae on Europa. *Icarus*, *271*, 49–56. https://doi.org/10.1016/j.icarus.2015.12.052

Dalton, J. B., Cassidy, T., Paranicas, C., Shirley, J. H., Prockter, L. M., & Kamp, L. W. (2013). Exogenic controls on sulfuric acid hydrate production at the surface of Europa. *Planetary and Space Science*, *77*, 45–63. https://doi.org/10.1016/j.pss.2012.05.013

Dalton, J. B., Prieto-Ballesteros, O., Kargel, J. S., Jamieson, C. S., Jolivet, J., & Quinn, R. (2005). Spectral comparison of heavily hydrated salts with disrupted terrains on Europa. *Icarus*, *177*(2), 472–490. https://doi.org/10.1016/j.icarus.2005.02.023

Fagents, S., Greeley, R., Sullivan, R. J., Pappalardo, R. T., Prockter, L. M., & Galileo SSI Team (2000). Cryomagmatic mechanisms for the formation of Rhadamanthys Linea, triple band margins, and other low-albedo features on Europa. *Icarus*, *144*(1), 54–88. https://doi.org/10.1006/icar.1999.6254

Fagents, S. A. (2003). Considerations for effusive cryovolcanism on Europa: The post-Galileo perspective. *Journal of Geophysical Research, Planets*, *108*(E12), 5139. https://doi.org/10.1029/2003JE002128

Figueredo, P. H., Chuang, F. C., Rathbun, J., Kirk, R., & Greely, R. (2002). Geology and origin of Europa's "Mitten" feature (Murias Chaos). *Journal of Geophysical Research*, *107*(E5), 5026. https://doi.org/10.1029/2001JE001591

Fink, U., Dekkers, N. H., & Larson, H. P. (1973). Infrared spectra of the Galilean satellites of Jupiter. *The Astrophysical Journal*, *179*, L155. https://doi.org/10.1086/181139

Fischer, P. D., Brown, M. E., Trumbo, S. K., & Hand, K. P. (2016). Spatially resolved spectroscopy of Europa's large-scale compositional units at 3-4 μm with Keck NIRSPEC. *The Astronomical Journal*, *153*(1), 13. https://doi.org/10.3847/1538-3881/153/1/13

Garcia-Baonza, V., Rull, F., & Dubessy, J. (2012). Raman spectroscopy of gases, water and related geological fluids. In J. Dubessy, M.-C. Caumon, & F. Rull (Eds.), *European Mineralogical Union Notes in Mineralogy*, (Vol. 12, pp. 279–320). Mineralogical Society of Great Britain and Ireland.

Genceli, F. E., Lutz, M., Spek, A. L., & Witkamp, G.-J. (2007). Crystallization and Characterization of a New Magnesium Sulfate Hydrate MgSO4 11H2O. *Crystal Growth & Design*, *7*(12), 2460–2466. https://doi.org/10.1021/cg060794e

Goodman, J. C., Collins, G. C., Marshall, J., & Pierrehumbert, R. T. (2004). Hydrothermal plume dynamics on Europa: Implications for chaos formation. *Journal of Geophysical Research, Planets*, *109*, E03008. https://doi.org/10.1029/2003JE002073

Greenberg, R. (1999). Chaos on Europa. *Icarus*, *141*(2), 263–286. https://doi.org/10.1006/icar.1999.6187

Greenberg, R., Geissler, P., Hoppa, G., Tufts, B. R., Durda, D. D., Pappalardo, R., et al. (1998). Tectonic processes on Europa: Tidal stresses, mechanical response, and Visible Features. *Icarus*, *135*(1), 64–78. https://doi.org/10.1006/icar.1998.5986

Greenberg, R., Leake, M. A., Hoppa, G. V., & Tufts, B. (2003). Pits and uplifts on Europa. *Icarus*, *161*(1), 102–126. https://doi.org/10.1016/S0019-1035(02)00013-1

Han, L., & Showman, A. P. (2008). Implications of shear heating and fracture zones for ridge formation on Europa. *Geophysical Research Letters*, *35*, L03202. https://doi.org/10.1029/2007GL031957

Hand, K. P., & Carlson, R. W. (2015). Europa's surface color suggests an ocean rich with sodium chloride. *Geophysical Research Letters*, *42*, 3174–3178. https://doi.org/10.1002/2015GL063559

Hanley, J., Dalton, J. B., Chevrier, V. F., Jamieson, C. S., & Barrows, R. S. (2014). Reflectance spectra of hydrated chlorine salts: The effect of temperature with implications for Europa. *Journal of Geophysical Research: Planets*, *119*, 2370–2377. https://doi.org/10.1002/2013JE004565

Hansen, G. B., & McCord, T. B. (2008). Widespread CO 2 and other non-ice compounds on the anti-Jovian and trailing sides of Europa from Galileo/NIMS observations. *Geophysical Research Letters*, *35*, L01202. https://doi.org/10.1029/2007GL031748

Head, J. W., & Pappalardo, R. T. (1999). Brine mobilization during lithospheric heating on Europa: Implications for formation of chaos terrain, lenticula texture, and color variations. *Journal of Geophysical Research, Planets*, *104*(E11), 27,143–27,155. https://doi.org/10.1029/1999JE001062

Head, J. W., Pappalardo, R. T., & Sullivan, R. (1999). Europa: Morphological characteristics of ridges and triple bands from Galileo data (E4 and E6) and assessment of a linear diapirism model. *Journal of Geophysical Research, Planets*, *104*(E10), 24,223–24,236. https://doi.org/10.1029/1998JE001011

Hogenboom, D. L., Kargel, J. S., Ganasan, J. P., & Lee, L. (1995). Magnesium sulfate-water to 400 MPa using a novel piezometer: Densities, phase equilibria, and Planetological Implications. *Icarus*, *115*(2), 258–277. https://doi.org/10.1006/icar.1995.1096

Jia, X., Kivelson, M. G., Khurana, K. K., & Kurth, W. S. (2018). Evidence of a plume on Europa from Galileo magnetic and plasma wave signatures. *Nature Astronomy*, *2*(6), 459–464. https://doi.org/10.1038/s41550-018-0450-z

Johnson, T. V., & McCord, T. B. (1971). Spectral Geometric Albedo of the Galilean Satellites, 0.3 to 2.5 Microns. *The Astrophysical Journal*, *169*, 589. https://doi.org/10.1086/151177

Kadel, S. D., Fagents, S. A., Greeley, R., & Galileo SSI Team (1998). *Trough-bounding ridge pairs on Europa: Considerations for an endogenic model of formation*. Houston, TX: Paper presented at Lunar and Planetary Science Conference XXIX.

Kadleíková, M., Breza, J., & Veselý, M. (2001). Raman spectra of synthetic sapphire. *Microelectronics Journal*, *32*(12), 955–958. https://doi.org/10.1016/S0026-2692(01)00087-8

Kargel, J. S. (1991). Brine volcanism and the interior structures of asteroids and icy satellites. *Icarus*, *94*(2), 368–390. https://doi.org/10.1016/0019-1035(91)90235-L

Kivelson, M. G., Khurana, K. K., Russell, C. T., Volwerk, M., Walker, R. J., & Zimmer, C. (2000). Galileo magnetometer measurements: A stronger case for a subsurface ocean at Europa. *Science*, *289*, 1340–1343. https://doi.org/10.1126/science.289.5483.1340

Manga, M., & Michaut, C. (2017). Formation of lenticulae on Europa by saucer-shaped sills. *Icarus*, *286*, 261–269. https://doi.org/10.1016/j.icarus.2016.10.009

Manga, M., & Wang, C.-Y. (2007). Pressurized oceans and the eruption of liquid water on Europa and Enceladus. *Geophysical Research Letters*, *34*, L07202. https://doi.org/10.1029/2007GL029297

Markham, A. E., & Kobe, K. A. (1941). The solubility of carbon dioxide in aqueous solutions of sulfuric and perchloric acids at 25°. *Journal of the American Chemical Society*, *63*(4), 1165–1166. https://doi.org/10.1021/ja01849a507

McCord, T. B., Hansen, G. B., Fanale, F. P., Carlson, R. W., Matson, D. L., Johnson, T. V., et al. (1998). Salts on Europa's surface detected by Galileo's near infrared mapping spectrometer. *Science*, *280*(5367), 1242–1245. https://doi.org/10.1126/science.280.5367.1242

McCord, T. B., Hansen, G. B., Matson, D. L., Johnson, T. V., Crowley, J. K., Fanale, F. P., et al. (1999). Hydrated salt minerals on Europa's surface from the Galileo near-infrared mapping spectrometer (NIMS) investigation. *Journal of Geophysical Research, Planets*, *104*(E5), 11,827–11,851. https://doi.org/10.1029/1999JE900005

Méndez, A. S. J., Muñoz-Iglesias, V., Izquierdo-Ruíz, F., & Prieto-Ballesteros, O. (2017). Salting-out phenomenon induced by the clathrate hydrates formation at high-pressure. *Journal of Physics: Conference Series*, *950*, 042042. https://doi.org/10.1088/1742-6596/950/4/042042

Michaut, C., & Manga, M. (2014). Domes, pits, and small chaos on Europa produced by water sills. *Journal of Geophysical Research: Planets*, *119*, 550–573. https://doi.org/10.1002/2013JE004558

Minceva-Sukarova, B., Sherman, W. F., & Wilkinson, G. R. (1984). The Raman spectra of ice (I h, II, III, V, VI and IX) as functions of pressure and temperature. *Journal of Physics C: Solid State Physics*, *17*(32), 5833–5850. https://doi.org/10.1088/0022-3719/17/32/017

Muñoz-Iglesias, V., Bonales, L. J., & Prieto-Ballesteros, O. (2013). pH and salinity evolution of Europa's brines: Raman spectroscopy study of fractional precipitation at 1 and 300 bar. *Astrobiology*, *13*(8), 693–702. https://doi.org/10.1089/ast.2012.0900

Muñoz-Iglesias, V., Prieto-Ballesteros, O., & Bonales, L. J. (2014). Conspicuous assemblages of hydrated minerals from the H2O–MgSO4–CO2 system on Jupiter's Europa satellite. *Geochimica et Cosmochimica Acta*, *125*, 466–475. https://doi.org/10.1016/j.gca.2013.10.033

Orlando, T. M., McCord, T. B., & Grieves, G. A. (2005). The chemical nature of Europa surface material and the relation to a subsurface ocean. *Icarus*, *177*(2), 528–533. https://doi.org/10.1016/j.icarus.2005.05.009

Pappalardo, R. T., & Barr, A. C. (2004). The origin of domes on Europa: The role of thermally induced compositional diapirism. *Geophysical Research Letters*, *31*, L01701. https://doi.org/10.1029/2003GL019202

Pappalardo, R. T., Belton, M. J. S., Breneman, H. H., Carr, M. H., Chapman, C. R., Collins, G. C., et al. (1999). Does Europa have a subsurface ocean? Evaluation of the geological evidence. *Journal of Geophysical Research, Planets*, *104*(E10), 24,015–24,055. https://doi.org/10.1029/1998JE000628

Pappalardo, R. T., Head, J. W., Greeley, R., Sullivan, R. J., Pilcher, C., Schubert, G., et al. (1998). Geological evidence for solid-state convection in Europa's ice shell. *Nature*, *391*(6665), 365–368. https://doi.org/10.1038/34862

Pelletier, M. J. (1999). Effects of temperature on cyclohexane Raman bands. *Applied Spectroscopy*, *53*(9), 1087–1096. https://doi.org/10.1366/0003702991947865

Pilcher, C. B., Ridgway, S. T., & McCord, T. B. (1972). Galilean satellites: Identification of water frost. *Science*, *178*(4065), 1087–1089. https://doi.org/10.1126/science.178.4065.1087

Portier, S., & Rochelle, C. (2005). Modelling CO2 solubility in pure water and NaCl-type waters from 0 to 300 °C and from 1 to 300 bar: Application to the Utsira Formation at Sleipner. *Chemical Geology*, *217*(3–4), 187–199. https://doi.org/10.1016/j.chemgeo.2004.12.007

Prieto-Ballesteros, O., Kargel, J. S., Fernández-Sampedro, M., Selsis, F., Martínez, E. S., & Hogenboom, D. L. (2005). Evaluation of the possible presence of clathrate hydrates in Europa's icy shell or seafloor. *Icarus*, *177*(2), 491–505. https://doi.org/10.1016/j.icarus.2005.02.021

Prockter, L. M., & Patterson, G. W. (2009). Morphology and evolution of Europa's ridges and bands. In R. T. Pappalardo, W. B. McKinnon, & K. Khurana (Eds.), *Europa*, (pp. 237–258). Tucson, TX: University of Arizona Press.

Qiao, E., & Zheng, H. (2017). Raman spectroscopic study of cyclohexane at pressures below 1000MPa. *Spectrochimica Acta Part A: Molecular and Biomolecular Spectroscopy*, *185*, 52–54. https://doi.org/10.1016/j.saa.2017.05.033

Quick, L. C., Glaze, L. S., & Baloga, S. M. (2017). Cryovolcanic emplacement of domes on Europa. *Icarus*, *284*, 477–488. https://doi.org/10.1016/j.icarus.2016.06.029

Quick, L. C., & Marsh, B. D. (2016). Heat transfer of ascending cryomagma on Europa. *Journal of Volcanology and Geothermal Research*, *319*, 66–77.

Rathbun, J. A., Musser, G. S., & Squyres, S. W. (1998). Ice diapirs on Europa: Implications for liquid water. *Geophysical Research Letters*, *25*, 4157–4160.

Roth, L., Saur, J., Retherford, K. D., Strobel, D. F., Feldman, P. D., McGrath, M. A., & Nimmo, F. (2014). Transient water vapor at Europa's south pole. *Science*, *343*(6167), 171–174. https://doi.org/10.1126/science.1247051

Rudolph, W. W., Irmer, G., & Hefter, G. T. (2003). Raman spectroscopic investigation of speciation in MgSO4(aq). *Physical Chemistry Chemical Physics*, *5*(23), 5253. https://doi.org/10.1039/b308951g

Sathyanarayana, D. N. (2004). *Vibrational spectroscopy: Theory and applications*. New Delhi: New Age International.

Schmidt, B. E., Blankenship, D. D., Patterson, G. W., & Schenk, P. M. (2011). Active formation of "chaos terrain" over shallow subsurface water on Europa. *Nature*, *479*(7374), 502–505. https://doi.org/10.1038/nature10608

Shenk, P. M., & McKinnon, W. B. (2001). *Topographic variability on Europa from Galileo stereo images*. Houston, TX: Paper presented at Lunar and Planetary Science Conference XXXII.

Sloan, E. D., & Koh, C. (2007). Clathrate hydrates of natural gases, *Third Edition*. CRC Press. https://doi.org/10.1201/9781420008494

Sotin, C., Head, J. W., & Tobie, G. (2002). Europa: Tidal heating of upwelling thermal plumes and the origin of lenticulae and chaos melting. *Geophysical Research Letters*, *29*(8), 1233. https://doi.org/10.1029/2001GL013844

Sparks, W. B., Hand, K. P., McGrath, M. A., Bergeron, E., Cracraft, M., & Deusta, S. E. (2016). Probing for evidence of plumes on Europa with HST/STIS. *The Astrophysical Journal*, *829*, 121. https://doi:10.3847/0004-637X/829/2/121

Sparks, W. B., Schmidt, B. E., McGrath, M. A., Hand, K. P., Spencer, J. R., Cracraft, M., & Deustua, S. E. (2017). Active cryovolcanism on Europa? *The Astrophysical Journal*, *839*(2), L18. https://doi.org/10.3847/2041-8213/aa67f8

Spaun, N. A., Pappalardo, R. T., & Head, J. W. (2001). *Equatorial distribution of chaos and lenticulae on Europa*. Houston, TX: Paper presented at Lunar and Planetary Science Conference XXXII.

Trumbo, S. K., Brown, M. E., Fischer, P. D., & Hand, K. P. (2017). A new spectral feature on the trailing hemisphere of Europa at 3.78 μm. *The Astronomical Journal*, *153*(6), 250. https://doi.org/10.3847/1538-3881/aa6d80

Walker, C. C., & Schmidt, B. E. (2015). Ice collapse over trapped water bodies on Enceladus and Europa. *Geophysical Research Letters*, *42*, 712–719. https://doi.org/10.1002/2014GL062405

Walrafen, G. E., Hokmabadi, M. S., & Yang, W. -H. (1986). Raman isosbestic points from liquid water. *The Journal of Chemical Physics*, *85*(12), 6964–6969. https://doi.org/10.1063/1.451383